Acta Polytechnica **66**(2):127–138, 2026
https://doi.org/10.14311/AP.2026.66.0127

Published by the Czech Technical University in Prague

EFFECT OF SYNTHETIC FIBRE ADDITION ON HEAT AND BALLISTIC RESISTANCE OF STEEL FIBRE-REINFORCED RPC

Martina Drdlová[a,*], Petr Bibora[a], Ingrid Khongová[a], Michael Pánek[a], Nikola Šuleková[b]

[a] *Research Institute for Building Materials, Hněvkovského 65, 617 00 Brno, Czech Republic*

[b] *Brno University of Technology, Faculty of Civil Engineering, Veveří 95, 602 00 Brno, Czech Republic*

[*] corresponding author: drdlova@vush.cz

Abstract. The study investigates the effect of synthetic fibre addition on the heat and ballistic resistance of steel fibre-reinforced reactive powder concrete (RPC). A comprehensive experimental programme was conducted involving prismatic (40 mm × 40 mm × 160 mm) and cylindrical (150 mm in diameter, 40 mm in height) specimens subjected to a range of elevated temperatures and ballistic impacts. Steel fibre-reinforced RPC specimens containing additional synthetic fibre reinforcement, namely polyethene terephthalate (PET), polyvinyl alcohol (PVA), and aromatic polyamide, which varied in geometry, were cast. The specimens were subjected to elevated temperatures ranging from 200 °C to 800 °C (in 200 °C increments with dwell time of 2–6 hours), and their residual compressive and flexural strength under quasi-static loading was then evaluated. Ballistic resistance was evaluated through depth of penetration (DOP) tests, which involved the impact of 7.62 × 54R B32 armour-piercing incendiary (API) projectiles at a striking velocity of 850 m s^{-1}. Differential efficiency factor (DEF), structural integrity, and impact crater dimensions were determined. The results show that the addition of PET and PVA fibres significantly improved the RPC's heat resistance, with PET fibres providing the highest residual strength and integrity after prolonged high-temperature exposure, while aramid fibres did not improve the thermal performance. Both PET and PVA fibres also markedly reduced the ballistic damage area and maintained high ballistic resistance after heating. The findings highlight the potential of steel-synthetic fibre hybridisation (especially with PET fibres) to design advanced RPC materials capable of withstanding combined ballistic and thermal threats, making them suitable for critical infrastructure and protective structures in extreme multi-hazard environments.

Keywords: RPC, reactive powder concrete, fibre, PET fibre, ballistic resistance.

1. Introduction

Reactive powder concrete is a type of ultra-high-performance concrete (UHPC) made using a mixture of fine aggregates, cement, silica fume, and superplasticisers in order to achieve exceptional strength and durability. The compressive and tensile strengths of RPCs typically exceed 150 MPa and 20 MPa, respectively, and fracture energy ranges from 12 to 40 kJ m^{-2} [1]. These exceptional mechanical parameters qualify RPC for use in structures with the potential to be subjected to extreme loading, such as blast and ballistic.

Steel fibres have been widely studied for their effectiveness in further improving the mechanical properties of RPC, including its capacity to resist high-velocity projectile impact or blast load. The fibres function as crack arresters, mitigating the propagation of cracks that could otherwise jeopardise the structural integrity of the material. Research demonstrates that steel fibres enhance penetration resistance by mitigating crack propagation and reducing spall damage [2–7]. For instance, incorporating steel fibres at 2 % by volume leads to an improvement in ballistic resistance, with a significant reduction in penetration depth and damage area [8, 9]. Furthemore, fibre orientation plays a critical role, with aligned fibres performing better under dynamic loads than random distributions [10]. Hybrid fibre reinforcement can provide superior high-strain rate characteristics and ballistic resistance compared to that of single-fibre reinforced UHPC, including RPC [8, 11]. The combination of steel and synthetic fibres reduces penetration depth and improves energy absorption under impact [12–16]. Nonetheless, the exploration of fibre reinforcement hybridisation in enhancing the ballistic resistance of Reactive Powder Concretes remains limited, with only a few combinations having been systematically investigated to date.

In real-world scenarios, extreme loads such as ballistic and blast impacts are frequently accompanied by fire, resulting in elevated temperatures. RPC's dense microstructure and low permeability make it prone to spalling, cracking, and loss of load-bearing capacity under fire exposure as a result of accumulated internal stresses from moisture evaporation. Hybrid fibre systems combining steel and synthetic fibres offer synergistic benefits, with steel fibres contributing to mechanical strength and synthetic fibres improving thermal performance. Adding synthetic fibres

Sample/ raw material	Cement [kg m^{-3}]	Sand [kg m^{-3}]	Silica fume [kg m^{-3}]	Quartz powder [kg m^{-3}]	SP [kg m^{-3}]	Water [kg m^{-3}]	Steel fibre [vol. %]	Polymer fibre type	Polymer fibre [vol. %]
RPC-REF	850	990	150	200	25	230	2	-	-
RPC-PET3	850	990	150	200	25	230	1.5	PET3	0.5
RPC-PET6	850	990	150	200	25	230	1.5	PET6	0.5
RPC-PVA3	850	990	150	200	25	230	1.5	PVA3	0.5
RPC-PVA6	850	990	150	200	25	230	1.5	PVA6	0.5
RPC-A3	850	990	150	200	25	230	1.5	A3	0.5
RPC-A6	850	990	150	200	25	230	1.5	A6	0.5

Table 1. Mix proportions of the RPC.

is an effective method to suppress the deterioration of RPC at high temperatures and enhance its thermal stability. These fibres act as sacrificial elements during fire exposure, creating micro-channels that relieve vapour pressure and prevent explosive spalling. Polypropylene (PP) fibres, in particular, are effective in improving spalling resistance when subjected to elevated temperatures, while the effect of polyethene (PE) is rather limited [17–23]. Experimental studies also reveal that the fibre dosage and type significantly influence the residual strength and structural integrity of RPC under high-temperature conditions [20, 23]. Lin [19] concluded that both PP and nylon fibres can inhibit high-temperature spalling of UHPC and ensure its corresponding mechanical properties. But it remains unclear how the fibre reinforcement optimised for enhancing the thermal resistance of Reactive Powder Concrete affects its ballistic resistance. The majority of existing studies in the literature examine these phenomena separately, focusing on a single type of load at a time. While this approach is justifiable due to the inherent complexity of each phenomenon, it does not fully reflect real-world conditions where these extreme loads often occur simultaneously. Studies evaluating the effect of the addition of polymer fibre reinforcement on both the ballistic and thermal performance of fibre-reinforced RPC are scarce, but results indicate that high ballistic and thermal properties can be achieved through hybrid reinforcement strategies [24, 25].

This study investigates the effects of incorporating synthetic fibres (PET, PVA, and aromatic polyamide) in varying geometries on the heat and ballistic resistance of reactive powder concrete, intending to offer deeper insights into its dual protective potential. The obtained data will help to design materials for structures with potential exposure to combined ballistic and thermal loads, such as structures of ammunition depots, military facilities, as well as critical infrastructures and other strategic buildings.

2. Materials and methods

2.1. Materials and mixing procedure

The main constituents of the steel fibre-reinforced RPCs used in this study were Portland cement CEM I 52.5 R produced by Aalborg (Denmark), and fine silica sand with a grain size of 0–0.5 mm (Střeleč, Czech Republic). Quartz powder with a mean grain size of 4 µm (Microdorsilit Chejn, Czech Republic) was used as a filler material. To achieve higher density and to increase the strength through pozzolanic reactions, undensified silica fume (Elkem 940 U, Norway) was added to the mixtures. Polycarboxylic superplasticiser Glenium ACE 430 (Master Builders Solutions, Germany) was used to reduce the need for mixing water. The mix proportions are given in Table 1. Steel fibres DM 6/0.17 produced by KrampeHarex (Germany) (6 mm in length, 0.17 mm in diameter) were used as the main fibre reinforcement. Polyethene terephthalate (PET) (Ciur, Czech Republic), polyvinyl alcohol (PVA) (Kuraray Europe, Germany), and aromatic polyamide (A) fibres (Teijin Frontier Europe, Germany) in two lengths (6 mm and 3 mm) were selected as secondary reinforcement in the presented study; their properties are listed in Table 2. Composition and properties of the cement used are listed in Tables 3 and 4.

The Hobart N50 mixer was used to mix the individual components. First, the dry ingredients were mixed for 2 minutes, then water with the superplasticiser was added, and the mixing continued for another 5 minutes. Steel, and subsequently polymer fibres, were added at the end of the mixing process. To remove the air entrained during the mixing procedure, the fresh mixtures were vacuum-treated for 2 minutes. After 25 hours of wet curing in the moulds, the specimens were demoulded and transferred to a water-filled tank to be cured for 28 days.

2.2. Methods

Prismatic specimens were subjected to thermal treatment (200 °C, 400 °C, 600 °C, and 800 °C, 2 dwell times – 2 and 6 hours) in a high-temperature electric muffle furnace (placed in a wire structure to provide distance between individual test specimens). The selected temperature interval was chosen to reflect both the typical thermal exposures experienced by concrete elements during severe fire events and the literature precedent, thereby ensuring that the results are both practically relevant and directly comparable to the majority of peer-reviewed studies in the field. A heating rate

Property	PET3	PET6	PVA3	PVA6	A3	A6
Material	Polyethylene terephthalate		Polyvinyl alcohol		Aramid	
Diameter [mm]	0.015	0.015	0.025	0.025	0.035	0.035
Length [mm]	3	6	3	6	3	6
Decomposition [°C]	255		200–230		400	
Coefficient of thermal expansion [$\times\frac{10^{-6}}{°C}$]	76.3	76.3	100	100	−3.5	−3.5
Tensile strength [MPa]	110	110	1 000	1 000	2 900	2 900
Specific gravity [kg m^{-3}]	1 350	1 350	1 300	1 300	1 400	1 400
Modulus of elasticity [GPa]	3	3	30	30	130	130

TABLE 2. Properties of the synthetic fibres.

Property	Value
Specific gravity [kg m^{-3}]	3.13
Specific surface – Blaine [m^2 kg^{-1}]	357
Compressive strength [MPa], 2, 7, 28 days	45, 60, 71
D50 [µm]	8.22

TABLE 3. Properties of the used cement.

Phase	Content [wt. %]
C_3S	72.0
C_2S	21.1
C_3A cubic	2.6
C_3A orthorhombic	0.6
C_4AF	0.2
$CaSO_4$	3.5

TABLE 4. Composition of the used cement.

of 5 °C min^{-1} was adopted. The universal strength testing machine TIRAtest 2710 was used to study the mechanical properties. Flexural and compressive strength tests were carried out at a loading rate of 0.2 kN s^{-1}. At least 5 test specimens for flexural strength and 10 test specimens for compressive strength were used for each mix. Bulk density was also determined. Additionally, selected specimens were subjected to Scanning Electron Microscopy (SEM) to investigate the microstructural changes and mechanisms underlying the observed macroscopic performance of the RPCs. The SEM analysis was performed using a scanning electron microscope Mira3, Tescan (Schottky Field Emission, with a max. resolution of 1 nm at 30 kV). The samples were coated with a 20 nm layer of AuPd. Secondary electron and Backscattered electron detectors were used simultaneously. To understand more deeply the changes occurring in the fibre-reinforced RPC under thermal stress, mercury porosimetry tests were performed on selected batches.

Ballistic resistance of the samples was evaluated on selected specimens via the Depth of penetration (DOP) test. This method assesses the ability of materials to withstand localised damage induced by projectile penetration, providing critical insights into their

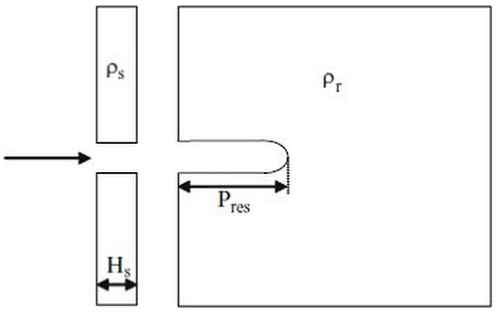

FIGURE 1. Scheme of DOP test.

mechanical performance under extreme loading conditions. During the test, the cylindrical specimen is mounted in a holder. The test setup is aligned to ensure that the projectile impacts the specimen perpendicular to its surface. The test induces a localised penetration and crater formation in the specimen. The primary objective of the DOP test is to quantify the residual penetration depth to which the projectile has penetrated the witness material located behind the test sample. In the presented study, a cylindrical test specimen (diameter of 150 mm, height of 40 mm) was positioned in front of a semi-infinite aluminium alloy witness material, characterised by its bulk density (ρ_r), and securely mounted on a stand. The test specimen was subjected to the impact of a 7.62 mm armour-piercing (AP) projectile with an approximate velocity of 850 m s^{-1}. Velocity sensors were implemented to confirm the projectile's striking speed. Following the impact, the penetration depth into the witness material was measured using X-ray imaging. The ballistic efficiency of the tested sample was calculated by comparing the projectile's penetration depth into the witness material with and without the sample in place. Using the sample's bulk density (ρ_s), thickness (H_s), and the reference penetration depth (P_r) of the projectile into the witness material without the sample, the differential efficiency factor (DEF) for each test was computed using Equation (1). This metric serves as a measure of the sample's ability to reduce projectile penetration and provides insights into its ballistic performance. The schematic of the DOP test is depicted in Figure 1.

Specimen	Bulk density [kg m $^{-3}$]	Compressive strength [MPa]	Flexural strength [MPa]
RPC-REF-20	2 490	198.6 ± 7.6	31.3 ± 3.1
RPC-REF-200-2	2 450	205.8 ± 5.4	18.4 ± 2.8
RPC-REF-400-2, RPC-REF-600-2, RPC-REF-800-2	Destroyed	Destroyed	Destroyed
RPC-A6-20	2 450	192.9 ± 4.6	37.7 ± 3.7
RPC-A6-200-2	2 400	196.0 ± 6.8	18.5 ± 3.4
RPC-A6-400-2, RPC- A6-600-2, RPC- A6-800-2	Destroyed	Destroyed	Destroyed
RPC-A3-20	2 435	195.2 ± 7.6	28.7 ± 2.9
RPC-A3-200-2	2 405	192.1 ± 5.6	13.1 ± 4.1
RPC-A3-400-2, RPC-A3-600-2, RPC-A3-800-2	Destroyed	Destroyed	Destroyed

Table 5. Physico-mechanical properties of the samples containing aramid fibres after exposure to elevated temperatures.

Specimen	Dwell time [h]	Bulk density [kg m $^{-3}$]	Compressive strength [MPa]	Flexural strength [MPa]
RPC-PET3-20	-	2 433	193.0 ± 5.75	32.0 ± 1.4
RPC-PET3-200-2	2	2 373	236.4 ± 17.7	21.7 ± 2.9
RPC-PET3-400-2	2	2 256	272.7 ± 14.1	18.3 ± 3.3
RPC-PET3-600-2	2	2 242	234.0 ± 11.2	14.4 ± 1.1
RPC-PET3-800-2	2	2 229	105.0 ± 1.5	8.2 ± 0.3
RPC-PET3-200-6	6	2 358	235.3 ± 9.4	15.8 ± 1.7
RPC-PET3-400-6	6	2 263	277.3 ± 10.9	14.9 ± 1.4
RPC-PET3-600-6	6	2 244	233.5 ± 11.4	16.0 ± 0.7
RPC-PET3-800-6	6	2 215	95.9 ± 5.21	7.7 ± 0.6
RPC-PET6-20	-	2 450	196.2 ± 9.5	33.2 ± 2.5
RPC-PET6-200-2	2	2 367	244.3 ± 7.6	21.1 ± 1.5
RPC-PET6-400-2	2	2 255	272.6 ± 23.1	23.0 ± 0.5
RPC-PET6-600-2	2	2 248	237.2 ± 9.2	15.8 ± 1.0
RPC-PET6-800-2	2	2 228	99.1 ± 8.36	8.5 ± 0.8
RPC-PET6-200-6	6	2 352	233.3 ± 9.4	19.0 ± 1.7
RPC-PET6-400-6	6	2 271	287.6 ± 10.9	17.5 ± 1.4
RPC-PET6-600-6	6	2 234	229.2 ± 11.4	16.7 ± 0.7
RPC-PET6-800-6	6	2 229	83.1 ± 5.2	7.2 ± 0.9

Table 6. Physico-mechanical properties of the samples containing PET fibres after exposure to elevated temperatures.

Equation (1) was used to determine the DEF:

$$\mathrm{DEF} = \frac{\rho_r \left(P_r - P_{\mathrm{res}}\right)}{\rho_s H_s}, \qquad (1)$$

where ρ_r is the bulk density of the witness material [kg m $^{-3}$], ρ_s is the bulk density of the test sample [kg m $^{-3}$], P_{res} is the residual penetration depth into the witness material after perforating the sample [mm], P_r is the penetration depth into the witness material without the sample [mm] and H_s is the thickness of the sample [mm].

Additionally, the depth of the crater was measured using callipers, and the area of the damaged surface was determined using the J-image software.

3. Results and discussion

3.1. Physico-mechanical parameters

The obtained values of bulk density, compressive and flexural strength of the mixtures are summarised in Tables 5–7. The photographic documentation of the specimens after the exposure to elevated temperatures is presented in Figure 2. The specimens are designated as follows: the number after the dash indicates the exposure temperature, and the following number indicates the dwell time. Example: RPC-A6-600-2 is the specimen containing 6 mm long aramid fibres, exposed to 600 °C for 2 hours.

Across all fibre types and lengths, bulk density decreased with increasing temperature, regardless of dwell time. This reduction is attributed to the evaporation of water (including bound water), and the degradation of the cementitious matrix from about 400 °C. REF samples and samples with aramid fibres were completely destroyed at higher temperatures (400 °C and above), indicating limited thermal resistance for this type of composite. PET and PVA fibre-reinforced samples exhibited a gradual loss of density, which stabilised at temperatures above 600 °C, suggesting better integrity under high-temperature exposure compared to REF and aramid fibre-reinforced RPCs.

Specimen	Dwell time [h]	Bulk density [kg m $^{-3}$]	Compressive strength [MPa]	Flexural strength [MPa]
RPC-PVA3-20	-	2 451	192.2 ± 7.8	31.1 ± 1.2
RPC-PVA3-200-2	2	2 370	220.3 ± 11.1	21.2 ± 1.1
RPC-PVA3-400-2	2	2 261	248.7 ± 9.1	19.2 ± 2.8
RPC-PVA3-600-2	2	2 238	174.4 ± 5.5	12.3 ± 0.3
RPC-PVA3-800-2	2	2 220	65.1 ± 6.3	6.4 ± 0.7
RPC-PVA3-200-6	6	2 365	217.1 ± 4.9	15.2 ± 1.4
RPC-PVA3-400-6	6	2 282	243.5 ± 7.1	15.6 ± 2.6
RPC-PVA3-600-6	6	2 225	166.1 ± 10.1	10.9 ± 3.2
RPC-PVA3-800-6	6	2 214	62.4 ± 11.1	6.7 ± 2.2
RPC-PVA6-20	-	2 440	187.4 ± 5.7	30.3 ± 1.6
RPC-PVA6-200-2	2	2 370	189.0 ± 9.5	20.7 ± 3.5
RPC-PVA6-400-2	2	2 250	236.2 ± 9.7	22.0 ± 1.2
RPC-PVA6-600-2	2	2 234	173.0 ± 8.2	19.2 ± 2.5
RPC-PVA6-800-2	2	2 220	76.1 ± 7.4	8.7 ± 1.8
RPC-PVA6-200-6	6	2 360	215.0 ± 9.1	17.9 ± 1.5
RPC-PVA6-400-6	6	2 262	247.6 ± 10.7	17.6 ± 2.2
RPC-PVA6-600-6	6	2 238	187.2 ± 7.5	14.0 ± 1.4
RPC-PVA6-800-6	6	2 222	62.1 ± 5.2	6.2 ± 0.7

TABLE 7. Physico-mechanical properties of the samples containing PVA fibres after exposure to elevated temperatures.

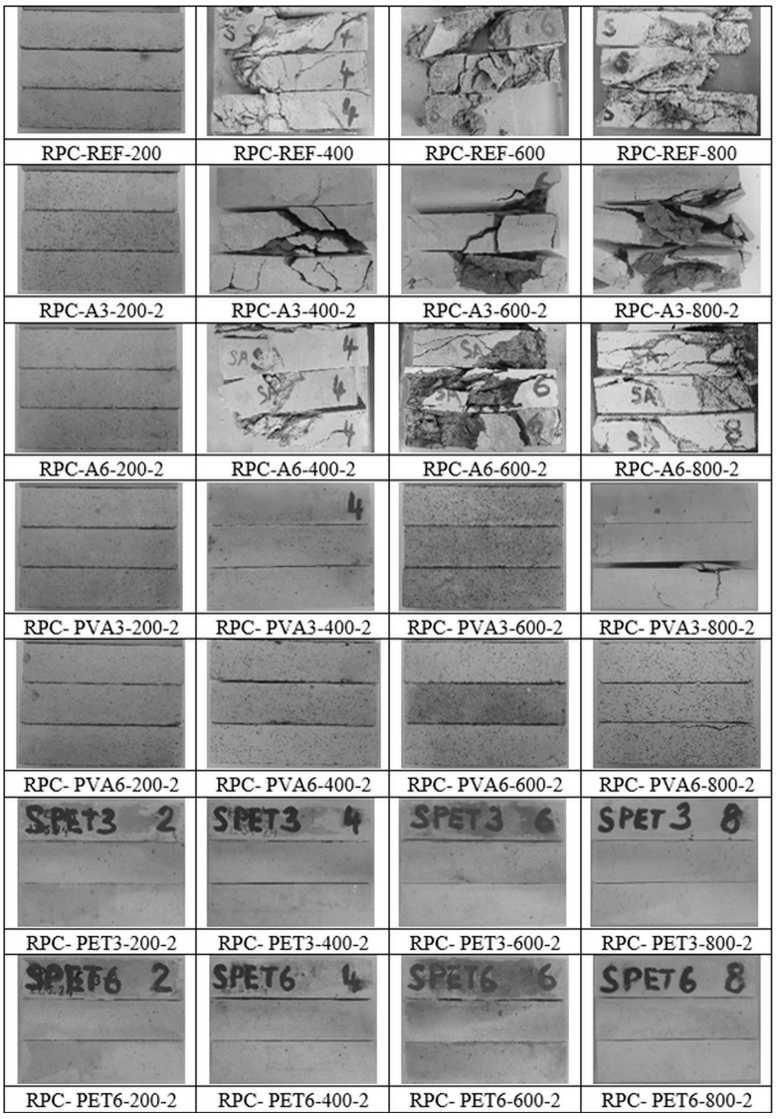

FIGURE 2. Photographic documentation of samples after thermal loading.

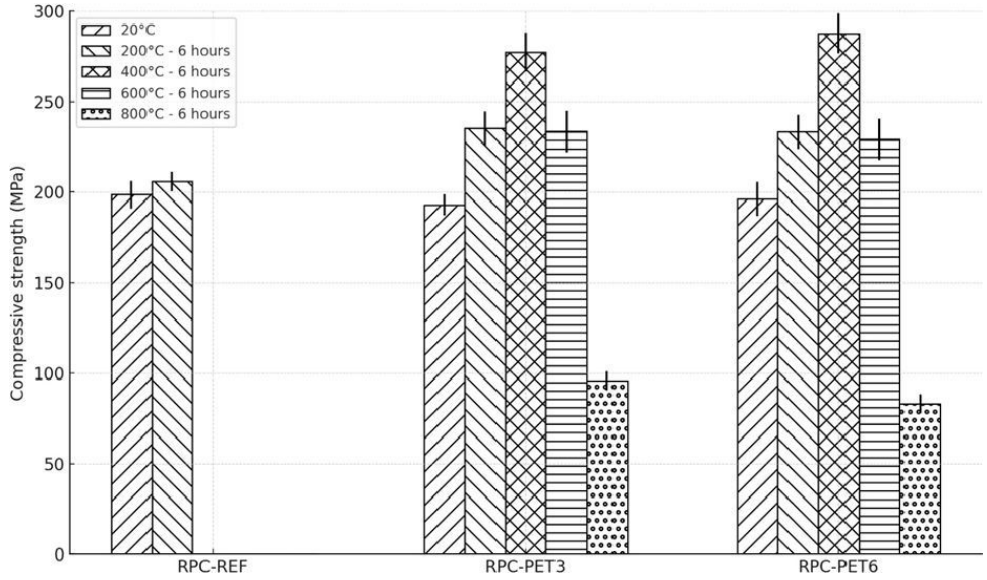

Figure 3. Trend in compressive strength of PET fibre reinforced samples with increasing exposure temperature.

The compressive strength of all the specimens at ambient temperature was slightly below 200 MPa, with no significant differences between the variants. At 200 °C, the compressive strength of the reference specimen increased slightly to 205.8 MPa, which is attributed to the densification of the matrix caused by the further hydration of previously unhydrated clinker, enabled by the moisture released through evaporation of free water. This behaviour aligns with the findings of Hiremath [17]. However, at higher temperatures (400 °C and above), the reference samples were completely destroyed. Intensive spalling occurred as a result of pore pressure build-up and thermal stress. Aramid fibre-reinforced specimens exhibited slightly lower compressive strengths compared to the reference specimens (192.9 MPa) at ambient temperature. At elevated temperatures, aramid fibre specimens demonstrated similar behaviour to reference ones. At 200 °C, aramid fibre-reinforced samples show a slight increase, at 400 °C and beyond, all aramid fibre-reinforced samples were completely destroyed. Photographic documentation of the samples after the thermal exposure is summarised in Figure 2.

All the samples containing PET fibres exhibited an initial increase at 200 °C, followed by a peak at 400 °C, and a subsequent decline at higher temperatures. In contrast to the reference sample and the samples containing aramid fibres, the samples containing PET fibres remained intact even after 6 hours of exposure to 800 °C. The addition of PET fibres significantly improved the heat resistance of RPC by creating escape routes for water vapour after their burnout. This contradicts the results published in study [19], in which no positive effect of adding PET fibres on the reduction of UHPFRC spallation was observed. However, in this study, fewer fibres were added (0.3 vol. %), which may not have been sufficient to create an effective network of channels for releasing vapour. At the strength peak, PET6 and PET3 samples exhibited an average increase in compressive strength of approximately 41 % and 43 %, respectively, compared to their compressive strength at ambient temperature. For a graphical representation of the trend of compressive strength development with increasing temperature (for samples with PET fibre inclusion and a temperature dwell of 6 h), see Figure 3. Similar observations were also reported in studies [1, 17]. The increase in strength can primarily be attributed to the densification of the cementitious matrix and the reduction in pore volume resulting from the further hydration of unreacted cement particles and the formation of an additional C-S-H gel [1, 17]. However, the partial filling of the burnt fibre channels with hydration products also contributes to the increase in strength, which will be further discussed in the following paragraphs.

As the temperature increases further, to between 600 °C and 800 °C, the compressive strength of the RPC containing PET3 and PET6 fibres drops. However, the values after exposure to 600 °C were still 21 % and 19 % higher, respectively, compared to corresponding samples at ambient temperature. The compressive strength reduction is related to the decomposition of calcium hydroxide and C-S-H and phase change of quartz, which leads to a significant loss of cohesion within the cement matrix, resulting in increased porosity and the propagation of microcracks. Furthermore, the thermal mismatch between the aggregates and the cement paste induces internal stresses, exacerbating damage and further undermining the concrete's structural integrity [1].

Longer dwell times (6 hours) generally resulted in slightly lower residual strengths compared to shorter dwell times (2 hours), particularly at higher temperatures. For example, RPC-PET6-0.5 retained a compressive strength of 233.5 MPa at 600 °C with a 6-hour dwell, compared to 237.2 MPa with a 2-hour dwell.

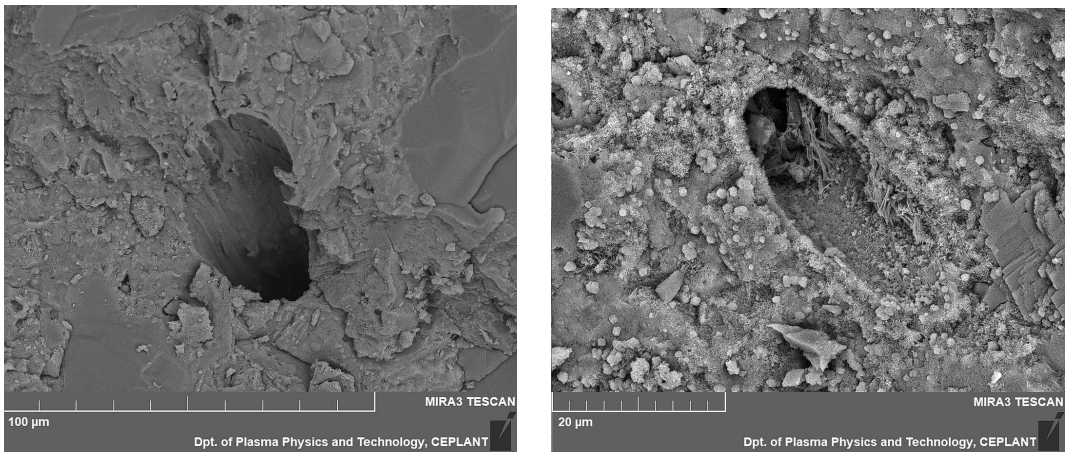

(A). RPC-PVA6. (B). RPC-PET6.

FIGURE 4. SEM image of channels after exposure to 400 °C: RPC-PVA6 with lower and RPC-PET6 with higher degree of filling with hydrated products.

Prolonged exposure thus increases thermal degradation, but relatively insignificantly within the observed exposure time. The fibre length had no effect on the residual strength; the values were identical for both fibre lengths within the measurement scatter.

The samples containing PVA fibres show the same trend with peak compressive strength at 400 °C, with generally lower values of compressive strength compared to samples containing PET fibres. At the strength peak, the samples containing PVA6 and PVA3 exhibited an average increase of approximately 28 % and 29 %, respectively, compared to the compressive strength at ambient temperature. The lower residual strength is an interesting finding that may help in the design of dual protection materials. The observed fact is caused by a combination of several phenomena occurring at the microstructural level. Firstly, it is related to the geometrical properties of the fibres. The PET fibres used in this study have a smaller diameter compared to PVA fibres (15 µm vs. 25 µm). As the polymer fibres burn out, the channels are gradually filled with higher-strength hydration products, eliminating porosity and strengthening the structure. As can be seen in Figure 4, the lower diameter channels are thus filled more with additional hydration products at 400 °C, which causes an increase in the overall compressive strength of the RPC at this temperature.

Another reason of the measured differences between PVA and PET fibre-reinforced samples can be the different microstructure of the materials after temperature exposure. The thermal expansion coefficients of synthetic fibres and cement matrix vary, resulting in thermal mismatch. This dissonance causes the synthetic fibres to expand radially around the cement matrix, forming microcracks along the fibre-matrix interface. The greater the difference in thermal expansion coefficients between the synthetic fibres and the cement matrix, the denser the microcrack network formed in the matrix by the synthetic fibres [19]. The coefficient of thermal expansion of PVA fibres differs from that of the cement matrix ($10 \times 10^{-6}\,°C^{-1}$) more than the coefficient of thermal expansion of PET, which may cause a higher number of created microcracks, weakening the structure and reducing the residual strength of the material. The higher level of deterioration on the microstructural level of the PVA samples was confirmed by SEM, as shown in Figure 5. Cracks can be observed at the edges of the channels for the PVA fibre specimen, while no cracks were detected for the PET fibre specimen.

Mercury intrusion porosimetry was employed to characterise the pore structure of RPC composites after the exposure to 400 °C for 6 hours. Figure 6 shows a comparison of the cumulative porosity and pore volume distributions of RPC reinforced with PET fibres and RPC reinforced with PVA fibres (both 6 mm in length). The PET fibre-reinforced RPC exhibits a more compact microstructure. The majority of pores is concentrated in the mesoporous range (10–100 nm), with a sharp decline in differential porosity above this range. This indicates a dense matrix with low total porosity, contributing to the high mechanical strength observed in earlier tests. The mercury porosimetry results support the explanation – based on SEM analysis – for the enhanced compressive strength of the PET-reinforced RPC at 400 °C, which is attributed to its lower porosity. The cumulative porosity of the PVA fibre-reinforced RPC is higher than that of the PET-modified counterpart. The RPC containing PVA fibres also exhibits a shift towards larger pore diameters – an increase in differential porosity was observed in the macropore range (>100 nm). This increased porosity is associated with reduced mechanical strength – as reflected by the lower residual compressive strength of PVA-reinforced samples. These porosimetry findings align with the SEM observations (Figure 5), which revealed partially filled voids (left behind after the thermal degradation) in PET samples and larger, unfilled channels and microcracks around the channels in PVA samples.

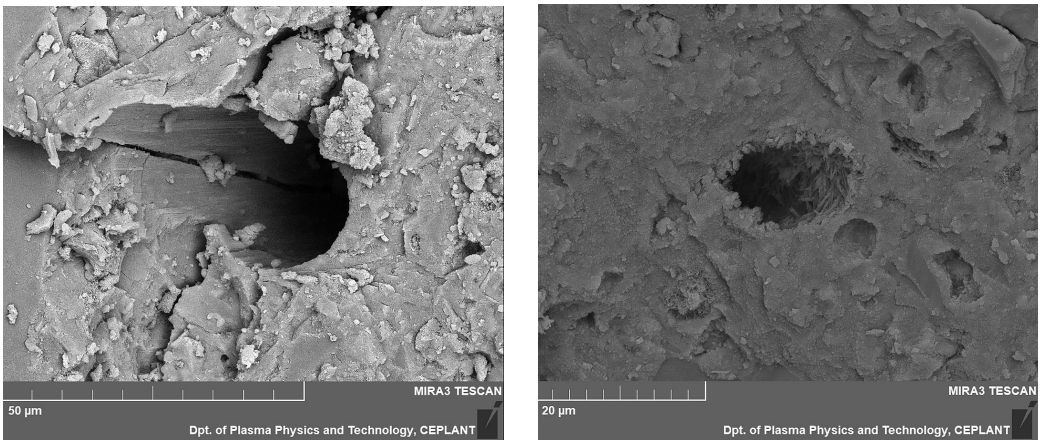

(a). RPC-PVA6. (b). RPC-PET6.

Figure 5. SEM of the microstructure of RPC-PVA6 and RPC-PET6 after exposure to 400 °C for 6 hours.

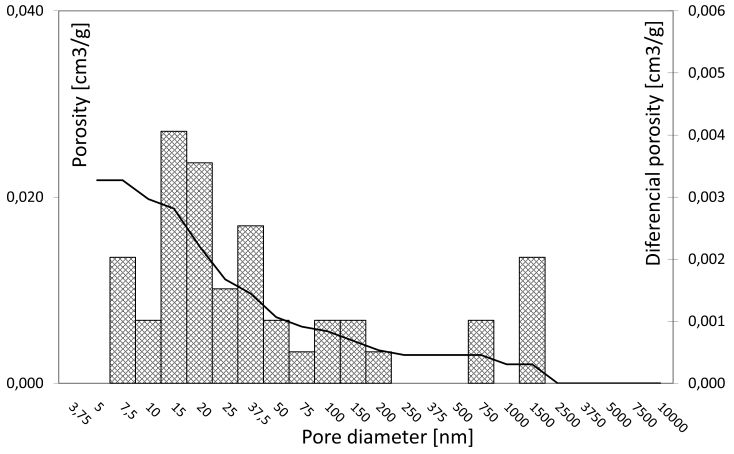

(a). RPC-PET6.

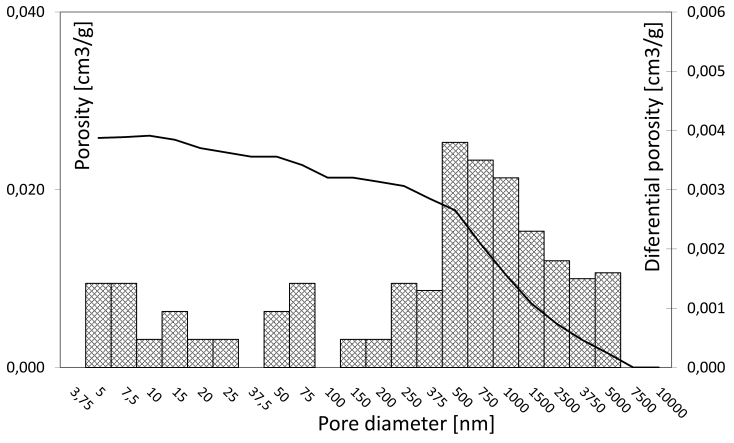

(b). RPC-PVA6.

Figure 6. Results of mercury porosimetry for RPC-PET6 and RPC-PVA6 after exposure to 400 °C for 6 hours.

The increase in compressive strength may also be connected to the higher melting point of the PET fibres, which enables them to retain their structural integrity for longer at elevated temperatures, reducing water release in the initial stage. This allows the matrix to benefit for longer from the internal "autoclave curing" of the high-strength matrix with a subsequent high strength gain, as previously reported in [26, 27].

Flexural strength At ambient temperature, adding synthetic fibres did not significantly affect the ultimate flexural strength of RPC; the values were within the scatter. This is due to the fact that the flexural strength is primarily determined by the dominant steel fibre reinforcement. In comparison to the reference group, only the RPC containing aramid fibres exhibited a noticeable improvement in flexural

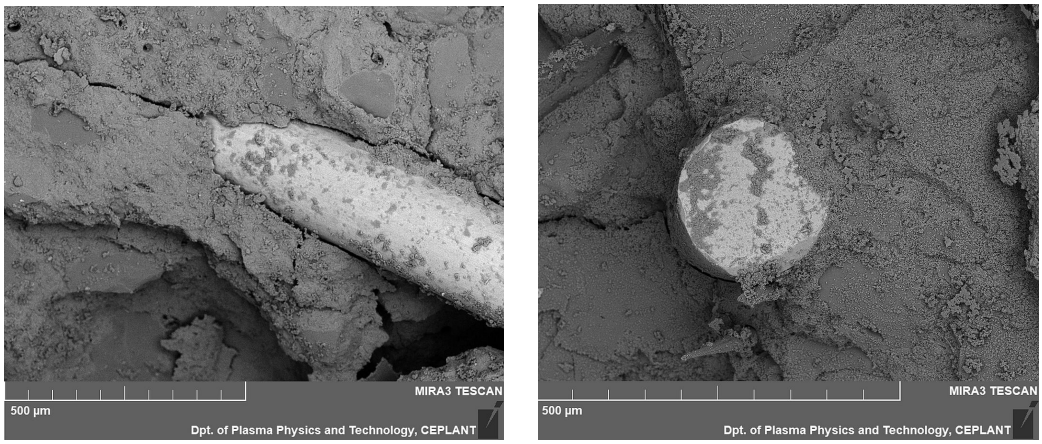

FIGURE 7. SEM image of microcracks developed around steel fibres after thermal exposure (200 °C).

Specimen	DEF [-]		h_{cr} [mm]		S [mm]	
	20 °C	600 °C	20 °C	600 °C	20 °C	600 °C
RPC-REF	0.949 ± 0.038	-	16.41 ± 1.32	-	$3\,921 \pm 634$	-
RPC-A3	0.943 ± 0.063	-	16.52 ± 1.28	-	$3\,765 \pm 655$	-
RPC-A6	0.951 ± 0.040	-	16.69 ± 1.87	-	$3\,655 \pm 955$	-
RPC-PET3	0.954 ± 0.044	0.961 ± 0.016	14.94 ± 1.40	14.53 ± 1.11	$1\,819 \pm 388$	$2\,529 \pm 328$
RPC-PET6	0.948 ± 0.078	0.956 ± 0.027	14.52 ± 2.13	14.68 ± 1.61	$2\,334 \pm 134$	$2\,505 \pm 435$
RPC-PVA3	0.942 ± 0.046	0.913 ± 0.041	15.20 ± 1.02	14.67 ± 1.12	$2\,790 \pm 298$	$3\,220 \pm 378$
RPC-PVA6	0.969 ± 0.044	0.934 ± 0.051	15.50 ± 0.91	15.12 ± 1.34	$3\,143 \pm 634$	$3\,315 \pm 420$

TABLE 8. Ballistic performance of RPC before and after exposure to elevated temperatures.

strength. The increase in the initial cracking strength of RPC containing aramid fibres can be attributed to their relatively high elastic modulus and tensile strength [28].

After exposure to elevated temperatures, the trends of residual flexural strength differed from those of compressive strength. A decrease was observed at 200 °C in all cases, followed by a similar strength value at 400 °C, and then another decrease at 600 °C, when similar values to those at 400 °C were reached. After 600 °C, the degradation of RPC flexural stiffness was the most pronounced. Obtained values were similar for both PVA and PET fibre samples after thermal exposure. Different fibre lengths did not affect the flexural strength of the test specimens after thermal exposure. The loss of flexural strength at temperatures as low as 200 °C can be explained by the difference in the thermal expansion coefficients of the cement matrix and the steel fibres, leading to the development of stresses at the fibre-matrix interface and microcrack formation, which reduces the cohesion and weakens the bridging effect of fibres when flexurally loaded. The microcrack development is shown in Figure 7.

Overall, in terms of resistance to elevated temperatures, the addition of PET fibres yields better results compared to PVA. However, PVA is also very effective in increasing the heat resistance of RPCs. In contrast, aramid fibres are completely ineffective in this respect due to their too high melting point.

3.2. Ballistic resistance

Ballistic resistance of the hybrid fibre-reinforced RPC was evaluated both at ambient temperature and after exposure to elevated temperatures. Calculated values of DEF, crater depth (h_{cr}), and surface damage area (S) of individual samples are summarised in Table 8 (average values of 8 measurements). Photographs of representative samples of each tested variant after the DOP test are shown in Figure 8, including the example of an X-ray radiograph of the backing witness cylinder for RPC-A6-20 (with marked penetration depth P_{res}).

The results for the samples at ambient temperature (20 °C) show a comparable performance in terms of DEF for all the samples. A minor decrease in the DEF parameter was expected as a result of the partial replacement of steel fibres, which have better strength characteristics and higher modulus, as well as the possible introduction of air (porosity) when adding fibres with very low diameter and high aspect ratio. However, it has been observed that the addition of polymeric fibres does not affect the DEF of the samples to a high extent – higher values (RPC-PET3, RPC-A6, RPC-PVA6) and lower values (RPC-A3, RPC-PET6, RPC-PVA3) of DEF were obtained compared to reference sample, but the difference was not significant and was within the scatter. When assessing the ballistic performance, in addition to DEF, crater depth (hcr) and damage zone area must also be taken into consideration. Low hcr and a smaller damaged zone area

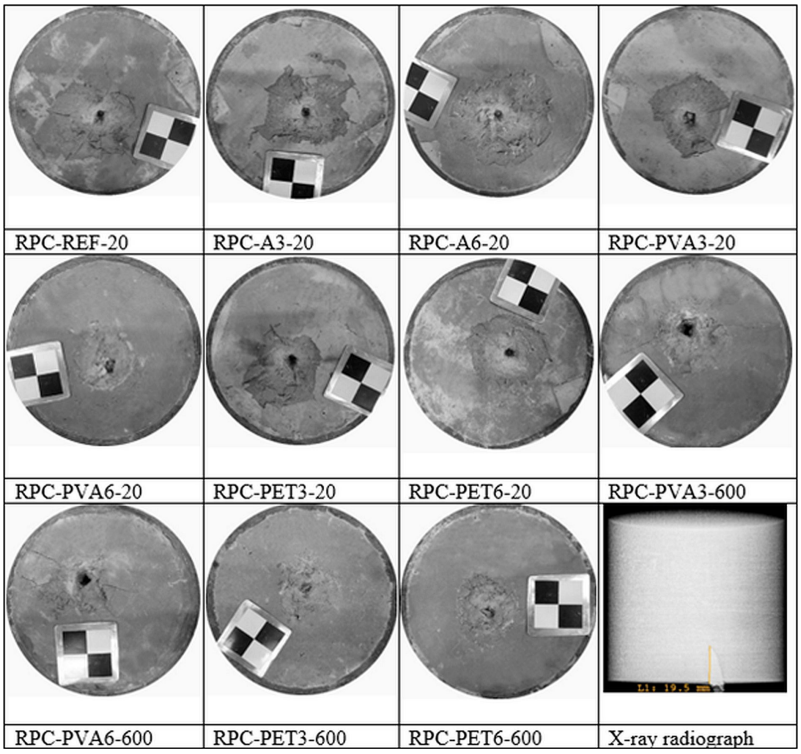

Figure 8. Representative samples of test bodies after the ballistic impact and the example X-ray radiograph of the backing witness cylinder with marked penetration depth (bottom right).

indicate reduced spalling and a lower risk of secondary fragments potentially hitting people in the vicinity [24]. When the original stress waves are induced by a projectile and propagate inwards, part of the imposed energy is consumed through fibre pull-out friction, elongation of fibres, and the bridging effect provided by the fibres. Adding 3 and 6 mm PET fibres led to a 53 % and 40 % reduction of the damaged zone, respectively. However, the secondary polymeric reinforcement was also effective in reducing the damaged area in the case of aramid and PVA fibres. This is attributed to the fact that all tested polymeric fibre variants have significantly lower fibre diameter and higher aspect ratio compared to steel fibres. At the same volume fraction, this results in a higher number of polymer fibres dispersed throughout the material. The increased fibre amount creates a more uniform reinforcement network and amplifies fibre-matrix contact areas, leading to enhanced local tensile strength, improved toughness, and reduced spalling and scabbing damage. This finding is consistent with previous research that has also reported on the effectiveness of such reinforcements in limiting damage propagation, as evidenced in studies examining the combined use of steel, aramid, and polypropylene fibres [16, 27], as well as steel and polypropylene fibre composites [29]. The effectiveness of a particular polymeric fibre reinforcement is not only related to its shape and mechanical parameters, but also to its ability to disperse and integrate into the cement matrix. Good results in suppressing spalling were achieved in the case of PVA3 and PVA6 fibres, with a reduction of the damaged area by 28 % and 20 %, respectively. This can be attributed primarily to the hydrophilic nature of this type of fibre and thus its good ability to adhere to the cement matrix. The significant reduction in surface damage area observed for PET fibres can be attributed to their shape parameters (fibre diameter is only 0.015 mm) and their good dispersibility (they do not clump together). They help to form a homogeneous material with a good ability to bridge microcracks and improve stress transfer. These fibres also have a rougher surface compared to aramid fibres, which improves their bonding.

Further ballistic tests were performed after exposure to 600 °C for six hours, the results of which are summarised in Table 8. The absence of data for RPC-REF, RPC-A3, and RPC-A6 at 600 °C means these samples failed to maintain structural integrity at 400 °C and above, and therefore were not tested. Comparing the PET- and PVA-reinforced samples, both samples containing PET or PVA fibres showed a high degree of ballistic resistance after the exposure. The DEF values of the PET-reinforced samples were even higher than that of the corresponding samples at room temperature, however, the increase is statistically insignificant. In the case of the PVA-reinforced samples, there was a minor decrease in DEF after temperature loading, but these values still indicate high ballistic resistance. The high temperatures caused a slight increase in the size of the damaged area, which is related to the embrittlement of the RPC due to the burnout of the polymer fibre reinforcement, the beginning of the decomposition of hydration products, and the modification of the quartz. The superior

ballistic resistance of the exposed PET fibre samples corresponds to the higher residual strengths observed during the evaluation of the quasi-static mechanical parameters of RPCs. This indicates that PET fibres (with specific tested shape parameters) are an effective means of achieving high ballistic resistance of the material at elevated temperatures. The inclusion of PET fibres creates favourable conditions for the further development of RPC strength at temperatures of up to 400 °C (the mechanisms were described in detail in Section 3.1), which subsequently translates into enhanced post-exposure strength and ballistic resistance. Further research is strongly recommended to investigate the influence of PET fibre parameters and quantities on the development of RPC strength at elevated temperatures, considering the initial strength of the material as well as the dimensions of the samples.

4. Conclusion

This study investigates the impact of adding synthetic fibres on the heat and ballistic resistance of steel fibre-reinforced reactive powder concrete (RPC). The major findings derived from the presented investigation are as follows:

- The results indicate that hybridisation of steel fibres with PET and PVA fibres significantly increases the heat resistance of RPC, with PET-reinforced samples exhibiting moderately better performance.
- Aramid fibres were ineffective in improving heat resistance due to their high thermal stability, which prevented the formation of vapour escape channels during thermal exposure.
- At ambient temperature, all hybrid fibre-reinforced RPC variants demonstrated comparable DEF to the reference specimen, indicating no significant reduction in ballistic resistance resulting from partial steel fibre replacement. On the contrary, PET and PVA fibres notably reduced the area of ballistic damage (spalling/scabbing), with PET fibres achieving a reduction in the damage zone of up to 53 %, thereby enhancing safety by minimising the risk of secondary fragments.
- No statistically significant differences were observed between the 3 mm and 6 mm fibre lengths for either PET or PVA fibres in terms of thermal or ballistic performance.
- The inclusion of both PET and PVA fibres significantly enhances the ballistic resistance of RPC after exposure to elevated temperatures (600 °C for 6 hours). The DEF values were comparable to those at ambient temperature, with overall better performance achieved by the sample with PET fibres.
- In order to optimise thermal resistance and post-heating ballistic performance, fibres with a lower diameter, a coefficient of thermal expansion closer to that of the matrix, and with good dispersibility, are the most suitable.

The presented findings provide valuable insights into the design of advanced materials for protective structures exposed to extreme, multi-hazard conditions.

Acknowledgements

This work was financially supported by the institutional support for the long-term conceptual development of research organisations provided by the Ministry of Industry and Trade of the Czech Republic.

References

[1] M. Abid, X. Hou, W. Zheng, R. R. Hussain. High temperature and residual properties of reactive powder concrete – A review. *Construction and Building Materials* **147**:339–351, 2017. https://doi.org/10.1016/j.conbuildmat.2017.04.083

[2] S. Ahmed, Z. Al-Dawood, F. Abed, et al. Impact of using different materials, curing regimes, and mixing procedures on compressive strength of reactive powder concrete – A review. *Journal of Building Engineering* **44**:103238, 2021. https://doi.org/10.1016/j.jobe.2021.103238

[3] P. Bibora, M. Drdlová, V. Prachař, O. Sviták. UHPC for blast and ballistic protection, explosion testing and composition optimization. *IOP Conference Series: Materials Science and Engineering* **251**(1):012004, 2017. https://doi.org/10.1088/1757-899X/251/1/012004

[4] H. Wei, T. Liu, A. Zhou, et al. Multiscale insights on enhancing tensile properties of ultra-high performance cementitious composite with hybrid steel and polymeric fibers. *Journal of Materials Research and Technology* **14**:743–753, 2021. https://doi.org/10.1016/j.jmrt.2021.07.001

[5] F. Zhang, L. H. Poh, M.-H. Zhang. Critical parameters for the penetration depth in cement-based materials subjected to small caliber non-deformable projectile impact. *International Journal of Impact Engineering* **137**:103471, 2020. https://doi.org/10.1016/j.ijimpeng.2019.103471

[6] H. Abbas, M. Al-Dabaan, N. Siddiqui, et al. Performance of reinforced concrete composite wall systems under projectile impact. *Journal of Materials Research and Technology* **23**:3062–3090, 2023. https://doi.org/10.1016/j.jmrt.2023.01.187

[7] N. Das, P. Nanthagopalan. State-of-the-art review on ultra high performance concrete – Ballistic and blast perspective. *Cement and Concrete Composites* **127**:104383, 2022. https://doi.org/10.1016/j.cemconcomp.2021.104383

[8] P. P. Li, H. J. H. Brouwers, Q. Yu. Influence of key design parameters of ultra-high performance fibre reinforced concrete on in-service bullet resistance. *International Journal of Impact Engineering* **136**:103434, 2020. https://doi.org/10.1016/j.ijimpeng.2019.103434

[9] J. Liu, C. Wu, Y. Su, et al. Experimental and numerical studies of ultra-high performance concrete targets against high-velocity projectile impacts. *Engineering Structures* **173**:166–179, 2018. https://doi.org/10.1016/j.engstruct.2018.06.098

[10] Y. Y. Y. Cao, P. P. Li, H. J. H. Brouwers, Q. L. Yu. Resistance of multi-layered UHPFRC against in-service projectile: Experimental investigation and modelling prediction. *Composite Structures* **244**:112295, 2020. https://doi.org/10.1016/j.compstruct.2020.112295

[11] M. Drdlová, P. Bibora, R. Čechmánek. Blast resistance of slurry infiltrated fibre concrete with hybrid fibre reinforcement. *IOP Conference Series: Materials Science and Engineering* **379**(1):012024, 2018. https://doi.org/10.1088/1757-899X/379/1/012024

[12] J. Feng, X. Gao, J. Li, et al. Influence of fiber mixture on impact response of ultra-high-performance hybrid fiber reinforced cementitious composite. *Composites Part B: Engineering* **163**:487–496, 2019. https://doi.org/10.1016/j.compositesb.2018.12.141

[13] M. Drdlová, P. Böhm, P. Bibora. Effect of production technology on high strain rate characteristics of reactive powder concrete. *Procedia Structural Integrity* **42**:1391–1397, 2022. https://doi.org/10.1016/j.prostr.2022.12.177

[14] J. Feng, X. Gao, J. Li, et al. Penetration resistance of hybrid-fiber-reinforced high-strength concrete under projectile multi-impact. *Construction and Building Materials* **202**:341–352, 2019. https://doi.org/10.1016/j.conbuildmat.2019.01.038

[15] J. Liu, J. Li, J. Fang, et al. Ultra-high performance concrete targets against high velocity projectile impact – a-state-of-the-art review. *International Journal of Impact Engineering* **160**:104080, 2022. https://doi.org/10.1016/j.ijimpeng.2021.104080

[16] T. Almusallam, A. Abadel, N. Siddiqui, et al. Impact behavior of hybrid-fiber reinforced concrete beams. *Structures* **39**:782–792, 2022. https://doi.org/10.1016/j.istruc.2022.03.062

[17] P. Hiremath, S. C. Yaragal. Performance of polypropelene and polyester fibres-reinforced reactive powder concretes at elevated temperatures. *Construction and Building Materials* **373**:130862, 2023. https://doi.org/10.1016/j.conbuildmat.2023.130862

[18] H. K. Sultan, I. Alyaseri. Effects of elevated temperatures on mechanical properties of reactive powder concrete elements. *Construction and Building Materials* **261**:120555, 2020. https://doi.org/10.1016/j.conbuildmat.2020.120555

[19] J. Lin, Y. Zhang, S. Huang, et al. Influence of synthetic fibers on the performance of ultra-high performance concrete (UHPC) at elevated temperatures. *Journal of Building Engineering* **97**:110735, 2024. https://doi.org/10.1016/j.jobe.2024.110735

[20] Y.-S. Tai, M.-H. Lee. Tensile behavior and damage mechanisms of ultra-high-performance concrete with blended steel fibers under elevated temperatures. *Journal of Building Engineering* **107**:112742, 2025. https://doi.org/10.1016/j.jobe.2025.112742

[21] M. X. Xiong, J. Y. R. Liew. Spalling behavior and residual resistance of fibre reinforced ultra-high performance concrete after exposure to high temperatures. *Materiales de Construcción* **65**(320):e071, 2015. https://doi.org/10.3989/mc.2015.00715

[22] J.-J. Park, D.-Y. Yoo, S. Kim, S.-W. Kim. Benefits of synthetic fibers on the residual mechanical performance of UHPFRC after exposure to ISO standard fire. *Cement and Concrete Composites* **104**:103401, 2019. https://doi.org/10.1016/j.cemconcomp.2019.103401

[23] S. Sriskandarajah, S. J. Foster. High temperature behaviour of hybrid steel – PVA fibre reinforced reactive powder concrete. *Materials and Structures* **49**(3):769–782, 2016. https://doi.org/10.1617/s11527-015-0537-2

[24] M. Drdlová, M. Šperl, D. Jančaříková, et al. Ballistic and heat resistance of hybrid-fiber reinforced reactive powder concrete. In V. Mechtcherine, C. Signorini, D. Junger (eds.), *Transforming Construction: Advances in Fiber Reinforced Concrete*, pp. 598–605. Springer Nature Switzerland, Cham, 2024. https://doi.org/10.1007/978-3-031-70145-0_72

[25] M. Boháč, D. Kubátová, M. Krejčí Kotlánová, et al. The role of SCM's on rheology of sprayed mortar. *IOP Conference Series: Materials Science and Engineering* **1039**(1):012001, 2021. https://doi.org/10.1088/1757-899X/1039/1/012001

[26] G.-F. Peng, X.-J. Niu, Y.-J. Shang, et al. Combined curing as a novel approach to improve resistance of ultra-high performance concrete to explosive spalling under high temperature and its mechanical properties. *Cement and Concrete Research* **109**:147–158, 2018. https://doi.org/10.1016/j.cemconres.2018.04.011

[27] T. Wang, M. Yu, J. Tian, et al. Residual properties of ultra-high performance concrete containing steel-polypropylene hybrid fiber exposed to elevated temperature at early age. *Journal of Building Engineering* **99**:111507, 2025. https://doi.org/10.1016/j.jobe.2024.111507

[28] M. Mára, R. Sovják, J. Fornůsek. Using textile aramid fabrics to increase the ballistic resistance of ultra-high-performance steel-fibre reinforced concrete. *Acta Polytechnica* **60**(6):486–492, 2020. https://doi.org/10.14311/AP.2020.60.0486

[29] T. H. Almusallam, N. A. Siddiqui, R. A. Iqbal, H. Abbas. Response of hybrid-fiber reinforced concrete slabs to hard projectile impact. *International Journal of Impact Engineering* **58**:17–30, 2013. https://doi.org/10.1016/j.ijimpeng.2013.02.005